

On the k Nearest-Neighbor Path Distance from the Typical Intersection in the Manhattan Poisson Line Cox Process

Konstantinos Koufos, Harpreet S. Dhillon, Mehrdad Dianati and Carl P. Dettmann

Abstract—In this paper, we consider a Cox point process driven by the Manhattan Poisson line process. We calculate the exact cumulative distribution function (CDF) of the path distance (L1 norm) between a randomly selected intersection and the k -th nearest node of the Cox process. The CDF is expressed as a sum over the integer partition function $p(k)$, which allows us to numerically evaluate the CDF in a simple manner for practical values of k . The distance distributions can be used to study the k -coverage of broadcast signals transmitted from a road side unit (RSU) at an intersection in intelligent transport systems (ITS). They can also be insightful for network dimensioning in urban vehicle-to-everything (V2X) systems, because they can yield the exact distribution of network load within a cell, provided that the RSU is located at an intersection. Finally, they can find useful applications in other branches of science like spatial databases, emergency response planning, and districting. We corroborate the applicability of our distance distribution model using the map of an urban area.

Index Terms—Manhattan Poisson line Cox process, spatial databases, stochastic geometry, vehicular networks.

I. INTRODUCTION

The development of the road network is a key component of urban planning because it greatly affects commuting efficiency, districting, emergency response dispatching, and first-aid services, to name but a few. Since the recent advent of wireless connectivity for pedestrians, and the ongoing proliferation of connected vehicles through vehicle-to-everything (V2X) systems, the road network is also the setting for several location-based e-services [1]. Exemplar applications could be electric vehicles querying over the internet for the nearest charging stations, and/or pedestrians searching with their smartphones for the closest available taxis [2]–[5].

A. Modeling road networks

The simplest models for urban road networks utilize just a set of vertices and edges [6], [7]. The vertices may represent junctions, the start/end points of roadways, critical locations where the speed limit or the travel direction changes, etc. Naturally, two vertices are connected by an edge if there is a straight link between them, giving rise to the adjacency matrix of the road network, which is not necessarily binary. The graph representation is enhanced by assigning weights to the edges, which might be proportional to the (average or minimum) travel time and fuel cost, along the road segment(s) that the edge represents. Algorithms exploring the graph have been also developed, e.g., the best-first search to identify the

nearest neighbors from a vertex and Dijkstra's algorithm to find the shortest paths, i.e., the sequence of edges of minimal aggregate cost between two non-adjacent vertices [8]. We will also utilize Dijkstra's algorithm with edge weights equal to the Euclidean distance of road segments while validating our distance distribution models with a real map.

Another line of research, particularly useful for emergency response planning, assumes that the edge weights are proportional to the length of the associated streets, and models random events along the edges. If these events represent points of emergency, the graph distance distributions, see [9], can reveal the intrinsic properties of the response system we need to build to combat all emergencies effectively. For instance, they can be used to infer the number of ambulances, medical personnel, etc. we have to deploy.

While certainly important, the graph-based approaches apply to specific road networks. Even though different cities can share common road graph properties [10], the graph-based models provide limited abstraction. Besides, due to the high complexity of graph-based routines, it is often impossible to model the road network very precisely. Also, the graph representation cannot answer questions pertinent to network planning, e.g., what is the minimum required intensity of charging stations, so that two of them are within a driving distance of one kilometer from a randomly chosen intersection, with probability at least 90%? This paper aims to bridge this gap. We argue that the mathematical tools of stochastic geometry, see [11] for an introduction, widely and successfully utilized during the past 15 years in the performance evaluation of random wireless communication networks, see [12]–[18], can also be insightful for urban road planning.

Unlike the graph-based methodology, the stochastic geometry framework does not consider a specific road network. Only the intensity of streets is available (or can be estimated). In addition, we assume that: (i) The road layout has a relatively regular structure, hence, a Manhattan Poisson line process (MPLP) is a realistic model for it, and (ii) the locations of points of interest (POI) or facilities, e.g., gas stations, events triggering police action, etc. follow a homogeneous Poisson point process (PPP) along each street. Under these assumptions, i.e., a Manhattan Poisson line Cox process (MPLCP) for the locations of POI, we will derive the path distance (L1 norm) distribution of the k nearest-neighbors (kNN) (or POI) from a randomly selected intersection. We have identified three potential applications, namely spatial database queries, districting, and urban vehicular ad hoc networks (VANETs),

where the kNN path distance distributions could be of use. We elaborate on them next.

B. Motivation and prior art

In the kNN query, a spatial database returns the locations of the k nearest objects, in terms of network distance, to the query point (or agent) [2]. Consider, for instance, a driver looking for the k nearest hotels (static objects) in terms of travel time, or a pedestrian querying for the k nearest vacant cabs (mobile objects). The agent reports its location, and the database solves the query using, e.g., a graph representation for the road network [3, Fig. 2].

Even with static objects, the graph dynamically changes due to varying traffic conditions, and the computational complexity can quickly explode, especially with frequent queries from mobile agents [4]. The server must continuously track and update the locations of the k nearest objects for all the agents. Because of that, neglecting the constraints imposed by the road network, and using just Minkowski distances to solve the kNN problem, especially for group queries, has not been abandoned [5]. The study in [2] has pointed out that the Euclidean distance is a lower bound to the network distance, and thus, we could use it to prune the search space in kNN queries. However, pruning based on a lower bound is not always effective. Therefore the calculation of the exact path distance distributions, as we will do in this paper, will be very helpful.

Apart from spatial databases, the kNN distance distributions can also be used in the planning of dispatching policies for emergency response services and districting [19]. In balanced district design, the road network of a metropolitan area is partitioned into smaller units (territories) which contain about the same expected number of road accidents so that the workload is divided equally among police departments [19]. Given the size of the districts, the kNN distributions can be used to calculate the probability that a police department can cover the k nearest emergencies under some probabilistic target time guarantees.

The ongoing deployment of 5G networks and the standardization activities for V2X communication, e.g., the transmission of cooperative awareness messages from the vehicles to the infrastructure [20], and the response of the latter with the collective perception message [21] have motivated the development of spatial models tailored to vehicular networks. Despite the fact that urban streets have finite lengths, line processes have been extensively used in wireless communication research to gain analytical insights into the network's performance [13]–[16]. The one- and two-dimensional PPPs are valid models for urban VANETs, in the high- and the low-reliability regime respectively [22]. As a result, the optimal transmission probability in VANETs modeled by Cox point processes is different than that calculated using the PPP [16]. To draw valid conclusions about the network's performance the road intersections must be modeled explicitly. For motorway VANETs, on the other hand, the superposition of one-dimensional (1D) point processes is sufficient [23]–[25].

The studies in [13]–[15] have used a Poisson line process to capture the random orientation of streets, and stationary

1D PPPs to model the locations of vehicles per street. In the resulting Poisson line Cox process Φ_c , the study in [13] has evaluated the distance distribution between an arbitrary point in the plane and the nearest point of Φ_c . This is essentially the serving distance distribution in a cellular vehicular network with nearest base station association, where the locations of base stations follow the two-dimensional PPP [14]. The study in [15] has derived the coverage probability for the typical receiver in a VANET and pointed out the conflicting effect of the intensities of the roads and vehicles. It has also solved for the distance distribution between the typical vehicle and the nearest vehicle of Φ_c . The study in [26] has used the MPLCP to model the locations of base stations in urban street microcells and calculated their distance distribution to the origin to study properties of the interference distribution. Finally, for some recent results on the reliability of inter-vehicle communication in urban streets of finite length, forming intersections and T-junctions, see [27].

Unfortunately, the above studies have measured the distances in the Euclidean (L2 norm) sense, even though the attenuation of wireless signals, especially in millimeter-wave frequencies, is better described by a street canyon model [28, Eq. (1)]. In this regard, the kNN Manhattan distance distributions will be useful in investigating the k -coverage of wireless signals, diffracted around buildings at road intersections as they propagate. We will use them to identify, e.g., how many vehicles within half a kilometer from an intersection can successfully receive broadcast safety messages with probability at least $q\%$? Thus far, the kNN distributions have been identified for Poisson and binomial processes see [29]–[31], without considering the deployment constraints due to the road layout. For $k = 1$, more general convex geometries like the n -sided polygon have been also investigated [32].

C. Contributions

The probability distribution function (PDF) of the shortest path between a random intersection and a point of the MPLCP has been recently calculated in [33]. In this paper, we will generalize this result to $k \geq 1$ nearest points. We present various methods to do that, and finally, we cast the solution as a sum over the integer partitions of k . The computational complexity of the suggested numerical algorithm is low, and the cumulative distribution functions (CDFs) can be easily obtained for practical values of k . Finally, it should be noted that the CDF of the distance between a random intersection and the k -th nearest point of the MPLCP can serve as a lower bound to the CDF of the distance between a random position of the road and the k -th nearest neighbor of the MPLCP. For $k=1$ both CDFs are computed in [33].

Section II formally introduces the MPLCP. Section III calculates the PDF of the total length L_t of line segments inside a Manhattan square, centered at a randomly selected road intersection. In Section IV, we calculate the moment generating function (MGF) of the random variable (RV) L_t , and in Section V we present a numerical algorithm which can be used to compute the CDF of the distance between an intersection and the k -th nearest point of the MPLCP.

In Section VI, we validate the suggested algorithm against simulations. We also use real data for the road network obtained from an urban area to demonstrate its improved performance against existing models based on the PPP. In Section VII, we conclude.

II. SYSTEM MODEL AND NOTATION

A line process, in layman's terms, is just a random collection of lines. If we limit our attention to undirected lines in the Euclidean plane, each line ℓ_i can be uniquely determined by the following parameters: the length $\rho_i \geq 0$ and the angle $\phi_i \in [-\pi, \pi]$, measured counter-clockwise, of the line segment being perpendicular to line ℓ_i and passing through the origin [11, Chapter 8.2.2]. Therefore a line process can be associated with a point process, and vice versa, where the line ℓ_i is uniquely mapped to the point $x_i \in \mathbb{R}^2$ with polar coordinates (ρ_i, ϕ_i) . The associated point process is often called the representation space of the line process.

Let us consider the realizations of two independent 1D PPPs of equal intensity λ , along the x and y axes, and construct the associated realization of vertical and horizontal lines. All points on the x axis give rise to vertical lines $\phi_i \in \{0, \pi\}$, and all points along the y axis correspond to horizontal lines $\phi_i \in \{-\pi/2, \pi/2\}$. This is known as the Manhattan Poisson line process (MPLP). It is a stationary and motion-invariant line process owing to the stationarity and motion-invariance of the PPP in the representation space. Its intensity, defined as the mean total length of lines per unit area, is equal to 2λ [11, Chapter 8.1].

Due to the fact that the contact distribution of the 1D PPP is exponential, the distances between neighboring intersections of a MPLP follow the exponential distribution too with rate λ . The set of horizontal lines is denoted by $\Phi_{lh} = \{L_{h1}, L_{h2}, \dots\}$, the set of vertical lines by $\Phi_{lv} = \{L_{v1}, L_{v2}, \dots\}$, and $\Phi_l = \{\Phi_{lh}, \Phi_{lv}\}$ is the resulting MPLP.

Let us assume that along each line there are facilities, e.g. gas stations, whose locations follow another 1D PPP of intensity λ_g . Conditionally on the realization of the line process, the locations of facilities are independent. Under these assumptions, the distribution of facilities becomes a stationary Cox point process, denoted by Φ_g , and driven by Φ_l . A Cox point process is in general a doubly-stochastic PPP where the intensity measure is itself random, and it is subsequently constructed in a two-step random mechanism. See [34, Chapters 3 and 4] for an introduction. In our case, a set of random lines parallel to the x, y axes is generated first, followed by the random locations of facilities along each line. The intensity of the MPLCP is $2\lambda\lambda_g$ [11].

In this paper, we will calculate the path distance (L1 norm or Manhattan distance) distribution between an arbitrary intersection of the MPLP and its k -th nearest facility. In our calculations, the width of the road is ignored, because it is negligible as compared to the expected distance between neighboring road intersections λ_g^{-1} . All roads are assumed bi-directional, and the locations of the facilities are constrained along the road network. Note that it is straightforward to extend the calculations for different intensities λ_h, λ_v between

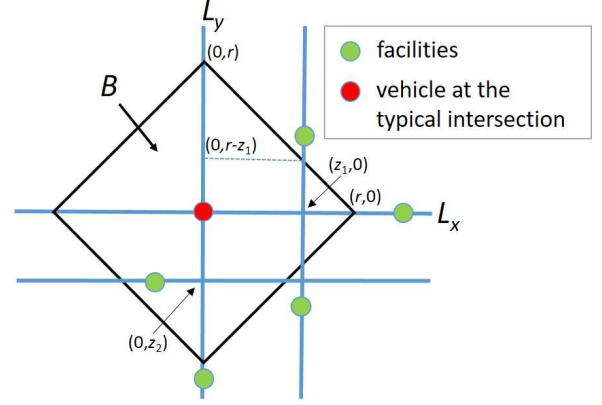


Fig. 1. Example realization of a MPLCP of facilities.

the vertical and horizontal streets. Consider for instance few main vertical streets traversing the city and many horizontal side streets. Unless otherwise stated, we will use $\lambda_h = \lambda_v = \lambda$ for presentation clarity.

Owing to the stationarity of the MPLP, we can add an intersection at the origin of the $x-y$ plane, and two (undirected) lines L_x, L_y passing through it, and aligned with the x and y axis respectively. Therefore under Palm probability, the resulting line process becomes $\Phi_L = \{\Phi_l \cup \{L_x, L_y\}\}$, and the point process of facilities is the superposition of the point process Φ_g and the two PPPs of intensity λ_g along L_x and L_y . See Fig. 1 for an illustration. Due to Slivnyak's Theorem [11, Chapter 8.2], the lines L_x, L_y does not affect the distribution of Φ_l . As a result, the distance distribution between a randomly selected intersection of Φ_l and its k -th nearest facility, is essentially equal to the distribution between the origin of the augmented grid Φ_L and its k -th nearest facility.

The CDF for the path distance of the k -th nearest facility to the origin is denoted by $F_{R_k}(r) = \mathbb{P}(R_k \leq r) = 1 - \mathbb{P}(R_k > r)$. The complementary CDF, $\mathbb{P}(R_k > r)$, is equal to the sum of the probabilities $P_j, j \in \{0, 1, 2, \dots, (k-1)\}$, hence, $F_{R_k}(r) = 1 - \sum_{j=0}^{k-1} P_j$, where P_j is the probability that there are exactly j facilities inside the square, see Fig. 1, which is the locus of points with Manhattan distance r to the origin. The set of all points inside the square, including the sides, is denoted by $B(r) \equiv B$ for brevity.

The CDF of the RV R_1 has been derived in [33, Theorem 1]

$$F_{R_1}(r) = 1 - P_0 = 1 - e^{-4\lambda_g r} e^{-4\lambda r(1-a_0)}, \quad (1)$$

where $a_0 = \frac{1-e^{-2\lambda_g r}}{2\lambda_g r}$ and $P_0 \triangleq e^{-4\lambda_g r} e^{-4\lambda r(1-a_0)}$ is the probability that no facility lies in B .

In addition, we define the RV $N_p(\Phi \cap B)$ which counts the number of points of the Cox process, driven by the line process Φ , within B . The total number of lines intersecting B , excluding the typical lines L_x, L_y is denoted by the RV N . Furthermore, the RV $L_i \geq 0$ describes the random length of the i -th line ℓ_i intersecting B , and the RV $L_t \geq 4r$ describes the total length of line segments in B including the contribution, $4r$, due to the typical lines. Finally, the realizations of the RVs L_i and L_t are both denoted by l .

III. CALCULATING P_k USING THE DISTRIBUTION OF L_t

Given the realization l of the RV L_t , the number of facilities in B follows a Poisson distribution with parameter $\lambda_g l$, $\text{Po}(\lambda_g l)$. As a result, based on the law of total expectation, the probability P_k that there are k facilities in B can be obtained by averaging the Poisson distribution over the PDF, $f_{L_t}(l)$, of the total length of line segments L_t in B . Hence,

$$P_k = \int_{4r}^{\infty} \frac{e^{-\lambda_g l} (\lambda_g l)^k}{k!} f_{L_t}(l) dl, \quad (2)$$

where the lower integration limit equals $4r$, because B always contains the segments due to the typical lines L_x, L_y .

In order to derive the PDF $f_{L_t}(l)$, we start with the random number N of line segments intersecting B , which follows the Poisson distribution with parameter $4\lambda r$. Recall that λ is the density of intersection points along a line, and $2r$ is the length of the diagonal of B . Conditionally on $N \geq 1$, the abscissas (ordinates) of the line segments parallel to L_y (L_x) are distributed uniformly at random in $(-r, r)$. As a result, the distribution of the RV L_i describing the length of the i -th line segment in B is uniform too. In order to derive its CDF, we note that L_i takes values in $(0, 2r)$ and thus, $\mathbb{P}(L_i \leq l) = \frac{l}{2r}$, $l \in (0, 2r)$. For instance, the vertical line with abscissa z_1 in Fig. 1 has length $l = 2(r - z_1)$ in B .

Conditionally on the realization $n \geq 1$ for the RV N , the total length of line segments in B , $\sum_{i=1}^n L_i$, is equal to the sum of n independent and identically distributed (i.i.d.) uniform RVs in $(0, 2r)$. As a result, the sum $\sum_{i=1}^n L_i$ follows the Irwin-Hall distribution with PDF

$$\sum_{i=1}^n L_i \sim \frac{1}{2r(n-1)!} \sum_{k=0}^{\lfloor \frac{l}{2r} \rfloor} (-1)^k \binom{n}{k} \left(\frac{l}{2r} - k \right)^{n-1}, \quad (3)$$

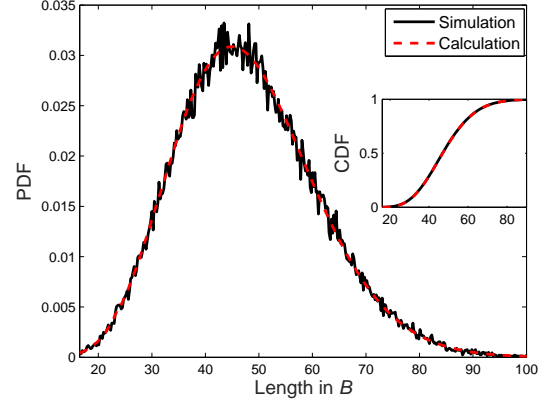
where $n \geq 1$ and $l \geq 0$.

In order to compute the PDF of L_t , we need to average equation (3) over the Poisson distributed number N for $n \geq 1$. The case $N = 0$, i.e., no intersections along $\{L_x \cup L_y\} \cap B$, which occurs with probability $e^{-4\lambda r}$, leads to $L_t = 4r$ and it is treated separately below.

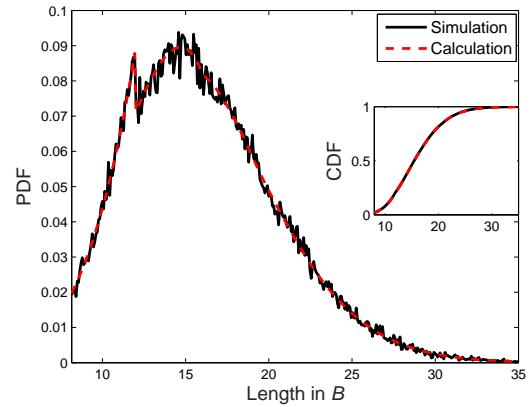
$$\begin{aligned} f_{L_t}(l) &= e^{-4\lambda r} \delta_{l,4r} + \\ &\mathbb{E}_{n \geq 1} \left\{ \frac{1}{2r(n-1)!} \sum_{k=0}^{\lfloor \frac{l-4r}{2r} \rfloor} (-1)^k \binom{n}{k} \left(\frac{l-4r}{2r} - k \right)^{n-1} \right\} \\ &= e^{-4\lambda r} \delta_{l,4r} + \sum_{n=1}^{\infty} \frac{(4\lambda r)^n e^{-4\lambda r}}{n!} \frac{1}{2r(n-1)!} \times \\ &\quad \sum_{k=0}^{\lfloor \frac{l-4r}{2r} \rfloor} (-1)^k \binom{n}{k} \left(\frac{l-4r}{2r} - k \right)^{n-1}, \quad l \geq 4r, \end{aligned} \quad (4)$$

where $\delta_{x,y} = 1$ for $x = y$ and $\delta_{x,y} = 0$ otherwise, is the Kronecker delta function, and also note that equation (3) has been shifted to the right by $4r$.

The above expression can be simplified, to some extent, by interchanging the order of summations, and while doing so,



(a) $\lambda = 0.5, r = 4$



(b) $\lambda = 0.5, r = 2$

Fig. 2. The PDF and the CDF (inset) of the total length L_t of line segments in B . In (b), the probability, $e^{-4\lambda r}$, that the only line segments are due to L_x, L_y is around 2%, evident in the left tail of the PDF. 10^5 simulations.

carefully setting the lower limit of the sum with respect to n . $f_{L_t}(l)$

$$\begin{aligned} &= e^{-4\lambda r} \delta_{l,4r} + \frac{e^{-4\lambda r}}{2r} \sum_{k=0}^{\lfloor \frac{l-4r}{2r} \rfloor} (-1)^k \times \\ &\quad \sum_{n=\max\{1, k\}}^{\infty} \frac{(4\lambda r)^n}{n!} \frac{1}{(n-1)!} \binom{n}{k} \left(\frac{l-4r}{2r} - k \right)^{n-1} \\ &= e^{-4\lambda r} \delta_{l,4r} + \frac{e^{-4\lambda r}}{2r} \left(4\lambda r {}_0F_1(2, 2\lambda(l-4r)) + \right. \\ &\quad \left. \sum_{k=1}^{\lfloor \frac{l-4r}{2r} \rfloor} (-1)^k \sum_{n=k}^{\infty} \frac{(4\lambda r)^n}{n!} \frac{1}{(n-1)!} \binom{n}{k} \left(\frac{l-4r}{2r} - k \right)^{n-1} \right) \\ &= e^{-4\lambda r} \delta_{l,4r} + \frac{e^{-4\lambda r}}{2r} \left(4\lambda r {}_0F_1(2, 2\lambda(l-4r)) + \right. \\ &\quad \left. \sum_{k=1}^{\lfloor \frac{l-4r}{2r} \rfloor} \frac{(-4\lambda r)^k}{k!} \left(\frac{l-4r}{2r} - k \right)^{k-1} {}_0F_1(k, 4\lambda r \left(\frac{l-4r}{2r} - k \right)) \right), \end{aligned} \quad (5)$$

where $l \geq 4r$ and ${}_0F_1(\alpha, z) = \sum_{k=0}^{\infty} \frac{1}{\Gamma(\alpha+k)} \frac{z^k}{k!}$ is the regularized hypergeometric function; example validations of equation (5) are depicted in Fig. 2.

The final expression in equation (5) is quite complicated to use in the integral in (2), hence, calling for another approach to evaluate the probabilities P_k .

IV. CALCULATING P_k USING MGFs

Since the PDF of the RV L_t has a complicated form, we may instead work with its MGF, $M_{L_t}(t) = \mathbb{E}\{e^{tL_t}\}$, $t \in \mathbb{R}$, which can be computed using the properties of the compound Poisson distribution. Recall that the RV L_t is equal to the sum of $N \sim \text{Po}(4\lambda r)$ i.i.d. uniform RVs $L_i \equiv L$ in $(0, 2r)$ plus the constant $4r$. Therefore,

$$\begin{aligned} \mathbb{E}\{e^{tL_t}\} &= \mathbb{E}_N\{\mathbb{E}\{e^{tL_t}|N\}\} \\ &= \mathbb{E}_N\{e^{4rt} M_L(t)^N\} \\ &\stackrel{(a)}{=} e^{4rt} \mathbb{E}_N\left\{\left(\frac{e^{2rt}-1}{2tr}\right)^N\right\} \\ &\stackrel{(b)}{=} \exp\left(4rt + 4\lambda r \left(\frac{e^{2rt}-1}{2rt} - 1\right)\right), \end{aligned} \quad (6)$$

where (a) follows from the MGF of a uniform RV, and (b) uses the probability generating function of a Poisson RV.

The limit of the first derivative of $M_{L_t}(t)$ with respect to t at $t \rightarrow 0$ in equation (6) yields $(4r + 4\lambda r^2)$, which is the mean of the RV L_t . The first term, $4r$, is the fixed length of the typical lines in B . The second term, $4\lambda r^2$ is, as expected, equal to the product of the mean length r of a randomly selected line segment L_i multiplied by the expected number $4\lambda r$ of line segments in B . Recall that the expected number of line segments is equal to the expected number of intersections along the typical lines.

Conditionally on the realization of the length $L_t = l$, the number of facilities in B is Poisson distributed with parameter $\lambda_g l$. As a result, using the law of total expectation, the MGF of the (discrete) RV of the number of facilities in B , $N_p(\Phi_L \cap B)$, can be read as

$$\begin{aligned} M_{N_p(\Phi_L \cap B)}(t) &= \mathbb{E}\{e^{N_p(\Phi_L \cap B)t}\} \\ &= \mathbb{E}_{L_t}\{\mathbb{E}\{e^{N_p(\Phi_L \cap B)t}|L_t\}\} \\ &\stackrel{(a)}{=} \mathbb{E}_{L_t}\{e^{\lambda_g l(e^t-1)}\} \\ &= M_{L_t}(\lambda_g(e^t-1)), \end{aligned}$$

where (a) is due to the MGF of a Poisson RV.

After substituting the above argument, $\lambda_g(e^t-1)$, into the last equality in (6), we obtain the MGF of the RV $N_p(\Phi_L \cap B)$. $M_{N_p(\Phi_L \cap B)}(t) =$

$$\exp\left(4r\lambda_g(e^t-1) + 4\lambda r \left(\frac{e^{2r\lambda_g(e^t-1)}-1}{2r\lambda_g(e^t-1)} - 1\right)\right).$$

Furthermore, starting from the definition of the MGF of a discrete RV on the natural numbers, $M_{N_p(\Phi_L \cap B)}(t) \equiv M_{N_p}(t) = \sum_{k=0}^{\infty} P_k e^{kt}$ we get P_k

$$\begin{aligned} &= \frac{1}{k!} \frac{d^k}{dt^k} M_{N_p}(\log t) \Big|_{t \rightarrow 0} \\ &= \frac{1}{k!} \frac{d^k}{dt^k} \exp\left(4r\lambda_g(t-1) + 4\lambda r \left(\frac{e^{2r\lambda_g(t-1)}-1}{2r\lambda_g(t-1)} - 1\right)\right) \Big|_{t \rightarrow 0}. \end{aligned} \quad (7)$$

After substituting $k = 0$ in equation (7), we obtain $P_0 = \exp(-4r\lambda_g - 4\lambda r(1-a_0))$, as expected, see equation (1). For $k=1$ in (7), after some simplification, we have

$$P_1 = P_0 (4r\lambda_g + 4r\lambda(a_0 - e^{-2r\lambda_g})). \quad (8)$$

The calculation of higher-order derivatives in (7) results in complicated expressions which are difficult to manipulate. For

instance, we list below the expressions we get, after some simplification, for P_2 and P_3 .

$$\begin{aligned} P_2 &= \frac{1}{2} P_0 (4r\lambda_g + 4r\lambda(a_0 - e^{-2r\lambda_g}))^2 + 4\lambda r P_0 \times \\ &\quad (a_0 - e^{-2r\lambda_g} - r\lambda_g e^{-2r\lambda_g}). \\ P_3 &= \frac{1}{6} P_0 (4r\lambda_g + 4r\lambda(a_0 - e^{-2r\lambda_g}))^3 + 4\lambda r P_0 \times \\ &\quad (4r\lambda_g + 4r\lambda(a_0 - e^{-2r\lambda_g})) \times \\ &\quad (a_0 - e^{-2r\lambda_g} - r\lambda_g e^{-2r\lambda_g}) + 4\lambda r P_0 \times \\ &\quad (a_0 - e^{-2r\lambda_g} - r\lambda_g e^{-2r\lambda_g} - \frac{2}{3} r^2 \lambda_g^2 e^{-2r\lambda_g}). \end{aligned} \quad (9)$$

One way to add some structure in the calculation of P_k , is to use the Faà di Bruno's formula, see for instance [35], for the calculation of the k -th derivative of a composite function. Let us define $f(t) = e^t$ and $g(t) = (4r\lambda_g(t-1) + 4\lambda r(\frac{e^{2r\lambda_g(t-1)}-1}{2r\lambda_g(t-1)} - 1))$, see equation (7). Leveraging on that $f^{(k)}(t) = e^t$, where $f^{(k)}$ denotes the k -th derivative, the Faà di Bruno's formula is simplified to [35, Eq. (2.2)]: $\frac{d^k f(g(t))}{dt^k}$

$$\begin{aligned} &= e^{g(t)} \sum_{m=1}^k B_{k,m}(g'(t), g''(t), \dots, g^{(k-m+1)}(t)) \\ &= e^{g(t)} B_k(g'(t), g''(t), \dots, g^{(k)}(t)), \end{aligned} \quad (10)$$

where $B_{k,m}$ and B_k are the partial and the complete exponential Bell polynomials respectively.

The Bell polynomials emerge in set partitions. For instance, $B_{4,2}(x_1, x_2, x_3, x_4) = 3x_2^2 + 4x_1x_3$, indicates that there are three ways to separate the set $\{x_1, x_2, x_3, x_4\}$ into two subsets of size two, and four ways to separate it into a block of size three and another of size one. Note that the total number of partitions, i.e., seven, is the Stirling number of second kind which, in general, counts the ways to separate an m -element set into k disjoint and non-empty subsets, e.g., $S(4, 2) = 7$. The calculation of the Bell polynomials is widely available in today's numerical software packages like Mathematica.

Recall from equation (7) that the k -th derivative of the MGF has to be evaluated in the limit $t \rightarrow 0$. It is also noted that $P_0 = e^{g(0)}$. Combining equations (7) and (10) yields

$$P_k = \frac{P_0}{k!} \sum_{m=1}^k B_{k,m}(g'(0), g''(0), \dots, g^{(k-m+1)}(0)). \quad (11)$$

Equation (11) above is insightful to understand why the calculation of P_3 in equation (9) consists of three terms. The first term over there, $(4r\lambda_g + 4r\lambda(a_0 - e^{-2r\lambda_g}))^3$, is essentially equal to the partial Bell polynomial $B_{3,3}(g'(0)) = g'(0)^3$. It is also straightforward to verify that the remaining two terms in (9) are equal to $B_{3,2}(g'(0), g''(0)) = 3g'(0)g^{(2)}(0)$ and $B_{3,1}(g'(0), g''(0), g^{(3)}(0)) = g^{(3)}(0)$.

The Faà di Bruno's formula can indeed provide some insight into the calculation of the MGF of the RV describing the total number of points in B , $N_p(\Phi_L \cap B)$, however, the cost of computing the k -order partial derivatives might be high, especially for large values of k . In the next section, we will use enumerative combinatorics, revealing a simple numerical algorithm to evaluate P_k without involving higher-order derivatives as in equation (11).

V. CALCULATING P_k USING INTEGER PARTITIONS

Let us assume there are k facilities in B and separate their allocation into two sets: along the typical segments L_x, L_y and in the rest of B . The probability $P_k = \mathbb{P}(N_p(\Phi_L \cap B) = k)$ can be read as $P_k =$

$$\sum_{i \leq k} \mathbb{P}(N_p(\{L_x \cup L_y\} \cap B) = i) \cdot \mathbb{P}(N_p(\Phi_L \cap B) = m), \quad (12)$$

where $(m = k - i)$, and the product of probabilities follows from the independent locations of intersections along L_x and L_y , and the independent locations of facilities along each line of Φ_L .

The first probability term in (12) can be calculated as $\mathbb{P}(N_p(\{L_x \cup L_y\} \cap B) = i)$

$$\begin{aligned} &= \mathbb{P}(N_p(L_x \cap B) + N_p(L_y \cap B) = i) \\ &\stackrel{(a)}{=} \frac{(4\lambda_g r)^i e^{-4\lambda_g r}}{i!}, \end{aligned} \quad (13)$$

where (a) uses the fact that the superimposed PPPs of facilities along L_x and L_y is another PPP with twice the intensity $2\lambda_g$.

The calculation of the second probability term in (12) is more involved, but similar to (13), it helps to consider just a single PPP of intersection points with twice the intensity, 2λ , along L_x instead of two line processes Φ_{lh}, Φ_{lv} . Let us denote the resulting distribution of vertical lines by Φ'_{lv} . Obviously, $\mathbb{P}(N_p(\Phi_L \cap B) = m) = \mathbb{P}(N_p(\{\Phi_{lv}, \Phi_{lh}\} \cap B) = m) = \mathbb{P}(N_p(\Phi'_{lv} \cap B) = m)$. The latter can be written as $\mathbb{P}(N_p(\Phi'_{lv} \cap B) = m)$

$$\begin{aligned} &= \sum_{n=0}^{\infty} \mathbb{P}(N_p(\Phi'_{lv} \cap B) = m | N = n) \cdot \mathbb{P}(N = n) \\ &= \sum_{n=0}^{\infty} \frac{(4\lambda r)^n e^{-4\lambda r}}{n!} \mathbb{P}(N_p(\Phi'_{lv} \cap B) = m | N = n). \end{aligned} \quad (14)$$

In order to calculate the conditional probability in (14), we have to enumerate the number of ways of allocating m facilities (or objects) into n lines (or urns), with both objects and urns being indistinct. For each possible allocation, we need to obtain its probability of occurrence, and finally we will sum over all obtained values. For $n \geq m$, the number of ways to allocate m objects into n urns is equal to the number of integer partitions of m , denoted by $p(m)$, because only the number of objects going to each urn is relevant. For $n < m$, the restricted integer partitions of size at most n , $p_n(m)$, have to be considered. Empty urns are obviously allowed. Next, we sum over the probabilities of all partitions. $\mathbb{P}(N_p(\Phi'_{lv} \cap B) = m | N = n) =$

$$\sum_{\xi \in p_n(m)} \mathbb{P}(N_p(\Phi'_{lv} \cap B) = m | N = n, \xi),$$

where $p_n(m) = p(m)$ for $n \geq m$ and ξ is the set associated with a partition, e.g., $p(3) = \{\{3\}, \{2, 1\}, \{1, 1, 1\}\}$.

After substituting the above equality in the last line of (14), and interchanging the orders of summations we end up with $\mathbb{P}(N_p(\Phi'_{lv} \cap B) = m) =$

$$\sum_{\xi \in p(m)} \sum_{n=|\xi|}^{\infty} \frac{(4\lambda r)^n e^{-4\lambda r}}{n!} \mathbb{P}(N_p(\Phi'_{lv} \cap B) = m | N = n, \xi), \quad (15)$$

where $|\cdot|$ denotes the set cardinality, e.g., $|\xi| = 2$ for $\xi = \{2, 1\}$.

At this point, it helps to define the parameter $a_k, k \in \mathbb{N}$ describing the probability that a vertical line with abscissa $z > 0$, uniformly distributed between the origin and the point $(r, 0)$, contains exactly k facilities in B , e.g., in Fig. 1, the line with abscissa z_1 does not contain any.

$$\begin{aligned} a_k &= \frac{1}{r} \int_0^r \frac{(2\lambda_g(r-z))^k}{\Gamma(k+1)} e^{-2\lambda_g(r-z)} dz \\ &= \frac{\Gamma(k+1, 2\lambda_g r)}{2\lambda_g r}, \end{aligned} \quad (16)$$

where $\Gamma(k+1) = k!$, $\Gamma(\alpha, x) = \frac{1}{\Gamma(\alpha)} \int_0^x t^{\alpha-1} e^{-t} dt$ is the lower incomplete Gamma function, and for $k = 0$ we obtain the parameter a_0 defined under equation (1).

Let us consider the partition $\xi = \{1, 1, \dots, 1\}$ with m 1's. The inner sum in equation (15), conditionally on this partition, yields $\mathbb{P}(N_p(\Phi'_{lv} \cap B) = m | \xi)$

$$\begin{aligned} &= \sum_{n=m}^{\infty} \frac{(4\lambda r)^n e^{-4\lambda r}}{n!} \cdot \mathbb{P}(N_p(\Phi'_{lv} \cap B) = m | N = n, \xi) \\ &= \sum_{n=m}^{\infty} \frac{(4\lambda r)^n e^{-4\lambda r}}{n!} \cdot \binom{n}{m} a_1^m a_0^{n-m} \\ &= \frac{(4\lambda r)^m a_1^m e^{-4\lambda r(1-a_0)}}{m!}, \end{aligned}$$

where the binomial coefficient $\binom{n}{m}$ represents the number of ways to select the m lines containing just one facility in B .

Substituting the above equation and equation (13) into (12) yields the conditional probability, $P_{k|\xi}$, of k facilities in $\{\Phi'_{lv} \cup L_x\} \cap B$ given the partition ξ .

$$\begin{aligned} P_{k|\xi} &= \sum_{i=0}^k \frac{(4\lambda_g r)^i e^{-4\lambda_g r}}{i!} \frac{(4\lambda r)^{k-i} a_1^{k-i} e^{-4\lambda r(1-a_0)}}{(k-i)!} \\ &= \frac{(4r(\lambda_g + \lambda a_1))^k P_0}{k!}. \end{aligned}$$

In a similar manner, we can evaluate $P_{k|\xi}$ for all $\xi \in p(k)$ and complete the calculation of $P_k = \sum_{\xi \in p(k)} P_{k|\xi}$ in (12). However, this might be cumbersome, unless a simple pattern is identified. Next, we will derive a simple expression for $P_{k|\xi}$, depending on the number of times an integer appears in the partition ξ . Let us consider $\xi = \{q, \dots, q, 1, \dots, 1\}$, where the q appears f times and there are also $(m - qf)$ 1's. The inner sum in equation (15), conditionally on the partition ξ with cardinality $|\xi| = ((m - qf) + f)$, yields $\mathbb{P}(N_p(\Phi'_{lv} \cap B) = m | \xi)$

$$\begin{aligned} &= \sum_{n=m-(q-1)f}^{\infty} \frac{(4\lambda r)^n e^{-4\lambda r}}{n!} a_q^f a_1^{m-qf} a_0^{n-(m-(q-1)f)} \times \\ &\quad \binom{n}{m-(q-1)f} \binom{m-(q-1)f}{f} \\ &= \binom{m-(q-1)f}{f} a_q^f a_1^{m-qf} \frac{(4\lambda r)^{m-(q-1)f} e^{-4\lambda r(1-a_0)}}{(m-(q-1)f)!}, \end{aligned}$$

where $|\xi| = (m - (q - 1)f)$ is the number of lines containing facilities in B . They are selected with $\binom{n}{m-(q-1)f}$ ways from the available n lines, and $\binom{m-(q-1)f}{f}$ is the number of ways to select f out of the segments containing facilities in B , and allocate q facilities to each one of them.

Keeping in mind that due to the existence of f replicas of the integer q in the partition, only up to $(k - qf)$ facilities

TABLE I
DETAILING THE CALCULATION OF P_5 USING INTEGER PARTITIONS. SEE
ALSO EQUATION (18).

Partition	Terms	Probability $P_{k \xi}$
$\{5\}$	$4\lambda r a_5$	$4\lambda r a_5 P_0$
$\{4, 1\}$	$4\lambda r a_4, 4r(\lambda_g + \lambda a_1)$	$16\lambda(\lambda_g + \lambda a_1)r^2 a_4 P_0$
$\{3, 2\}$	$4\lambda r a_3, 4\lambda r a_2$	$16\lambda^2 r^2 a_2 a_3 P_0$
$\{3, 1, 1\}$	$4\lambda r a_3, \frac{1}{2}(4r(\lambda_g + \lambda a_1))^2$	$32\lambda(\lambda_g + \lambda a_1)^2 r^3 a_3 P_0$
$\{2, 2, 1\}$	$\frac{1}{2}(4r\lambda a_2)^2, 4r(\lambda_g + \lambda a_1)$	$32\lambda^2(\lambda_g + \lambda a_1)r^3 a_2^2 P_0$
$\{2, 1, 1, 1\}$	$4r\lambda a_2, \frac{1}{6}(4r(\lambda_g + \lambda a_1))^3$	$\frac{128}{3}\lambda(\lambda_g + \lambda a_1)^3 r^4 a_2 P_0$
$\{1, 1, 1, 1, 1\}$	$\frac{1}{120}(4r(\lambda_g + \lambda a_1))^5$	$\frac{128}{15}(\lambda_g + \lambda a_1)^5 r^5 P_0$

may be located along L_x , we substitute the above equation and (13) into (12), ending up with

$$P_{k|\xi} = \sum_{i=0}^{k-1} \frac{(4\lambda_g r)^i e^{-4\lambda_g r}}{i!} \binom{k-i-(q-1)f}{f} a_q^f a_1^{k-i-1} \times \frac{(4\lambda r)^{k-i-(q-1)f} e^{-4\lambda r(1-a_0)}}{(k-i-(q-1)f)!} = \frac{(4r(\lambda_g + \lambda a_1))^{k-fq}}{(k-fq)!} \frac{(4\lambda r a_q)^f}{f!} P_0. \quad (17)$$

It is straightforward to generalize the above calculation to include partitions with more than one $q > 1$. Let us assume that the integer $q_i > 1$ appears $f_i \geq 1$ times in the partition ξ . Equation (17) can be generalized as

$$P_{k|\xi} = \frac{(4r(\lambda_g + \lambda a_1))^{k-\sum_i f_i q_i}}{(k-\sum_i f_i q_i)!} P_0 \cdot \prod_{q_i} \frac{(4\lambda r a_{q_i})^{f_i}}{f_i!}. \quad (18)$$

To sum up, in order to evaluate $P_{k|\xi}$, we start with $P_{k|\xi} = P_0$. Given that the integer $q > 1$ appears in the partition $f \geq 1$ times, we set $P_{k|\xi} \leftarrow P_{k|\xi} \frac{(4\lambda r a_q)^f}{f!}$. For $q = 1$, we set $P_{k|\xi} \leftarrow P_{k|\xi} \frac{(4r(\lambda_g + \lambda a_1))^f}{f!}$. We update $P_{k|\xi}$ for all integers $q \in \xi$. Next, we repeat the same procedure for all partitions ξ , and we compute the probability $P_k = \sum_{\xi \in p(k)} P_{k|\xi}$.

For illustration purposes, in Table I, we list the contributions of the seven different terms involved in the calculation of P_5 . The inputs in the rightmost column, which is equal to the product of the terms in the middle column, are generated based on equation (18). For instance, for the partition $\{3, 2\}$ we have $f_1 = f_2 = 1$, because each of the numbers $q_1 = 2, q_2 = 3$ appears only once in the partition. Furthermore, $(f_1 q_1 + f_2 q_2 = 5)$ and thus, the exponent of the term $(\lambda_g + \lambda a_1)$ is zero. Therefore, equation (18) degenerates to the product of just two terms, $4\lambda r a_2$ and $4\lambda r a_3$, scaled by P_0 , and the result for the probability $P_{5|\{3,2\}}$ directly follows.

Now, it becomes clear in the calculation of P_3 in equation (9) that the first term corresponds to the partition $\{1, 1, 1\}$ with $a_1 = a_0 - e^{-2r\lambda_g}$, the second term to the partition $\{2, 1\}$ with $a_2 = a_0 - e^{-2r\lambda_g} - r\lambda_g e^{-2r\lambda_g}$, and the last term to the partition $\{3\}$ with $a_3 = \frac{1}{2}(a_0 - e^{-2r\lambda_g} - r\lambda_g e^{-2r\lambda_g} - \frac{2}{3}r^2\lambda_g^2 e^{-2r\lambda_g})$. For completeness, the pseudocode used to calculate P_k is provided as Algorithm 1. Given $P_j, \forall j \in \{0, 1, \dots, (k-1)\}$, the CDF of the distance distribution is evaluated as $F_{R_k}(r) = 1 - \sum_{j=0}^{k-1} P_j$.

Thus far, we have considered equal intensity of intersections $\lambda_v = \lambda_h = \lambda$ along the typical lines L_x, L_y . The calculations

Algorithm 1 Compute P_k

```

1:  $a_q \leftarrow \frac{\Gamma(q+1, 2\lambda_g r)}{2\lambda_g r}, q = 0, 1, \dots, (k-1)$ 
2:  $P_0 \leftarrow e^{-4\lambda_g r - 4\lambda r(1-a_0)}, P_k \leftarrow 0$ 
3:  $\Xi = \text{IntegerPartitions}(k)$ 
4: for all  $\xi \in \Xi$  do
5:    $P_{k|\xi} \leftarrow P_0$ 
6:   for all  $q \in \xi$  do
7:      $f_q \leftarrow \text{card}_\xi(q)$ 
8:     if  $q = 1$  then
9:        $P_{k|\xi} \leftarrow P_{k|\xi} \frac{(4(\lambda_g + \lambda a_1)r)^{f_q}}{f_q!}$ 
10:    else
11:       $P_{k|\xi} \leftarrow P_{k|\xi} \frac{(4\lambda a_q r)^{f_q}}{f_q!}$ 
12:    end if
13:  end for
14:   $P_k \leftarrow P_k + P_{k|\xi}$ 
15: end for
```

in Algorithm 1 can be easily generalized to $\lambda_v \neq \lambda_h$. Specifically, one will have to use

$$P_0 \leftarrow e^{-4\lambda_g r - 2(\lambda_v + \lambda_h)r(1-a_0)}, \quad (19)$$

in line 2, and

$$P_{k|\xi} \leftarrow P_{k|\xi} \frac{(2(2\lambda_g + (\lambda_v + \lambda_h)a_1)r)^{f_q}}{f_q!}, \quad (20)$$

$$P_{k|\xi} \leftarrow P_{k|\xi} \frac{(2(\lambda_v + \lambda_h)a_q r)^{f_q}}{f_q!},$$

in lines 9 and 11 respectively. Also, the intensity of intersections for the full Manhattan grid can be read as $\lambda = \frac{2\lambda_v \lambda_h}{\lambda_v + \lambda_h}$.

VI. NUMERICAL ILLUSTRATIONS & APPLICATIONS

In this section, we will start by validating Algorithm 1 with simulations, and we will proceed with the study of three example scenarios where this Algorithm might be of use. Finally, we will show that Algorithm 1 can give a short and accurate estimate about the distance distributions in real road networks with an approximate regular street layout. For that, we will use the map of an area near Manhattan in New York with the map data retrieved using OpenStreetMap [36], [37].

In Fig. 3 we have validated the calculation of the path distance distribution using Algorithm 1 for the ten nearest neighbors of a MPLCP $k \leq 10$. Fig. 4 illustrates that the Euclidean distance (L2 norm) is a bad approximation to the Manhattan distance (L1 norm) distribution for a MPLCP. The approximation quality deteriorates for a larger k . The planar PPP of equal intensity, $\mu = 2\lambda\lambda_g$, where the locations of facilities are not constrained by the road network, is not a better approximation either. Note that for the PPP, the distance to the k -th nearest neighbor follows the generalized gamma distribution with PDF [38, Theorem 1]:

$$f_{R_k}(r) = \frac{2e^{-\mu\pi r^2} (\mu\pi r^2)^k}{r\Gamma(k)}. \quad (21)$$

Having justified that the planar PPP and the Euclidean distances are not good approximations to the path distances, we will next present some case studies where the path distance distributions can be of use.

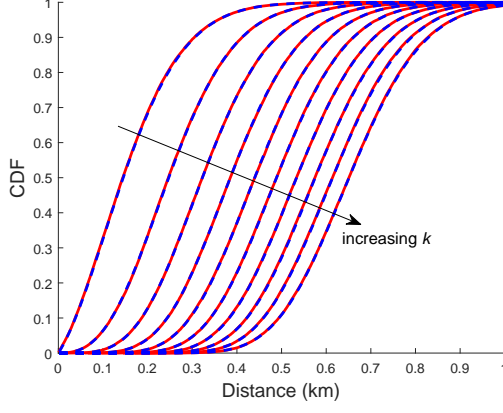


Fig. 3. The distance distributions for the k nearest facilities to the origin $k \in \{1, 2, \dots, 10\}$ following a MPLCP with dense streets $\lambda = 10 \text{ km}^{-1}$ and sparse facilities $\lambda_g = 0.5 \text{ km}^{-1}$. The red lines are averages over 50 000 simulations and the dashed blue lines are (exact) calculations using Algorithm 1. The simulations are carried out within a square area of 400 km^2 . The typical intersection (origin) is placed at the middle of the square. In each simulation, an independent realization of the MPLCP is generated and the path distances from the origin to the k nearest points of the process are computed. Note that in the calculation of P_9 , Algorithm 1 should go through 30 partitions but the computational complexity still remains very low.

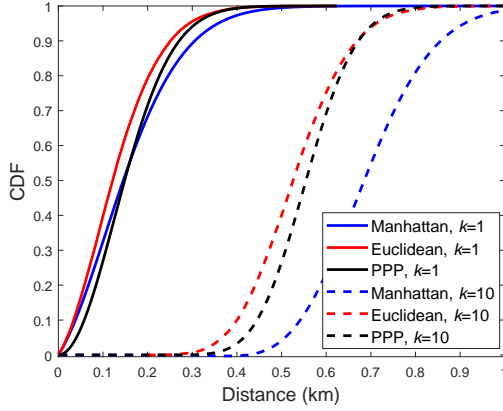


Fig. 4. The k -th nearest neighbor distance distributions $k \in \{1, 10\}$ from a random intersection, for a MPLCP with $\lambda = 10 \text{ km}^{-1}$ and $\lambda_g = 0.5 \text{ km}^{-1}$, using the Manhattan and the Euclidean distance. The associated distance distributions for a planar PPP of equal intensity are also demonstrated. The curves are generated using Algorithm 1 for the Manhattan distance, simulations for the Euclidean distance and equation (21) for the PPP.

A. Distance distributions in spatial database queries

Let us consider an electric vehicle at an intersection querying for the nearest charging station. The charging stations might be closed or fully occupied, depending on the time of day and the road traffic conditions. In that case, the spatial database should respond to the query by returning the *nearest available* charging station to the vehicle. The distance distributions developed in this paper can be used to calculate the path distance distribution and the distribution of travel time to the *nearest available* facility. Given that any facility is available with probability q , independently of other facilities, and the average travel speed is v , the CDF of the average travel time to the *nearest available* facility follows from the

geometric distribution:

$$\mathbb{P}(t \leq \tau) = \sum_{i=1}^{\infty} q(1-q)^{i-1} F_{R_i}(\tau), \quad (22)$$

where $\tau = rv^{-1}$.

See Fig. 5a for the validation of (22). Note that the underlying assumption in equation (22) is that the delay at the intersection and the traffic-related delays are not modeled explicitly but are incorporated into the model through the average velocity v .

B. Planning the network of facilities in a city

Before starting to build charging stations for electric vehicles in a city, it is important to identify their required density, i.e., the minimum number of stations per square kilometer, so that certain design constraints are satisfied. This process resembles network dimensioning in wireless communications. Given the intensity of roads λ , we would like to identify the minimum required intensity of facilities λ_g so that a vehicle at a randomly selected intersection can arrive at the nearest available facility within the target time, e.g., 100 s with probability larger than 90%. Due to the low computational complexity of the path distance distributions using Algorithm 1, we can obtain the required intensity λ_g numerically. To give an example, for the parameter settings used to generate Fig. 5b, the above target can be safely met for $\lambda_g \geq 1 \text{ km}^{-1}$.

C. Urban vehicular communication networks

Turning our interest to wireless communications applications, we assume that a RSU is deployed at the typical intersection and the locations of vehicles follow a MPLCP. The RSU broadcasts messages to the vehicles. For wireless propagation along urban street micro cells, the pathloss model should be different for line- and non-light-of-sight (NLoS) vehicles [39, Fig. 5]. The vehicles with NLoS connections suffer from serious diffraction losses due to the propagation of wireless signals around the corner. In Fig. 6 the distribution of the signal-to-noise ratio (SNR) for the 10 nearest vehicles with NLoS connection to the RSU is depicted. Assuming a distance-based propagation pathloss $r^{-\eta}$, where r stands for the Manhattan distance, and a diffraction loss \mathcal{L} , it is straightforward to convert the distance distributions into received signal level distributions. Then, it also remains to scale the obtained CDFs by the noise power level N_0 . Specifically, for the k -th nearest vehicle with NLoS connection we have

$$\begin{aligned} \mathbb{P}(\text{SNR}_k \leq \theta) &= \mathbb{P}(\mathcal{L}R_k^{-\eta} \leq \theta N_0) \\ &= 1 - \mathbb{P}\left(R_k \leq (\theta N_0 / \mathcal{L})^{-1/\eta}\right) \\ &= \sum_{j=0}^{k-1} \sum_{\xi \in p(j)} P_{j|\xi} \Big|_{r=(\theta N_0 / \mathcal{L})^{-1/\eta}}, \end{aligned} \quad (23)$$

where the vehicles along L_x, L_y with a line-of-sight connection to the RSU are neglected, hence, (18) degenerates to

$$P_{k|\xi} = e^{-4\lambda r(1-a_0)} \cdot \prod_{q_i} \frac{(4\lambda r a_{q_i})^{f_i}}{f_i!}.$$

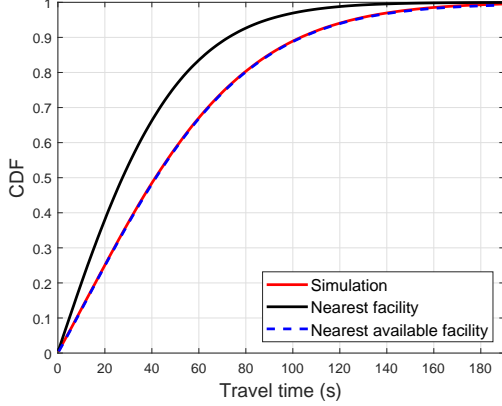
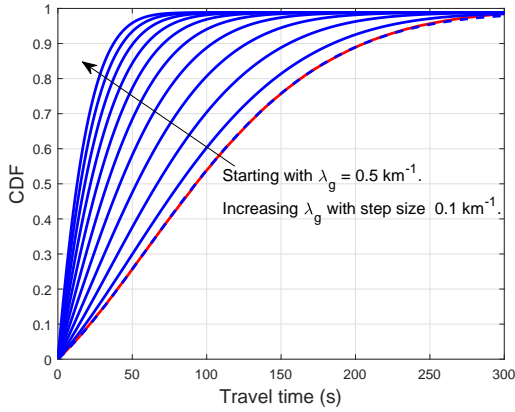
(a) $q = 0.6$ (b) $q = 0.2$

Fig. 5. Distribution of travel time to the nearest available facility from an intersection. Each facility is available with probability q independently of other facilities. $\lambda = 1 \text{ km}^{-1}$, $\lambda_g = 0.5 \text{ km}^{-1}$, $v = 10 \text{ m/s}$. The sum in (22) is truncated at $i = 20$ and validated against the simulations.

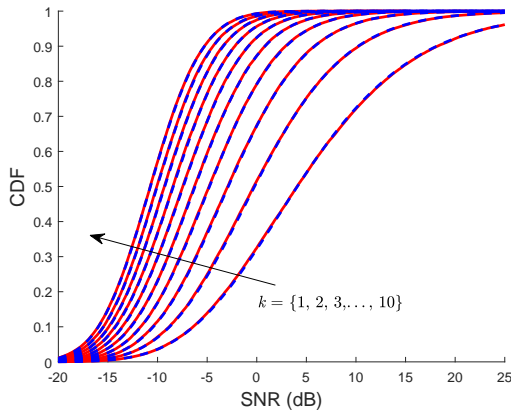


Fig. 6. The SNR distribution at the k nearest vehicles $k \leq 10$ with NLoS connection to the RSU. The locations of vehicles follow a MPLCP with $\lambda = 5 \text{ km}^{-1}$ and $\lambda_g = 10 \text{ km}^{-1}$. Distance-based pathloss $r^{-\eta}$ with $\eta = 3$, diffraction loss around the corner 20 dB and noise power level $N_0 = 10^{-8}$. The simulations are depicted in 'red' and the (exact) calculations in 'blue'.

Given the size of the cell B , see Fig. 1, it is straightforward to convert the distance distributions for the NLoS vehicles into the distribution of their number inside the cell – network

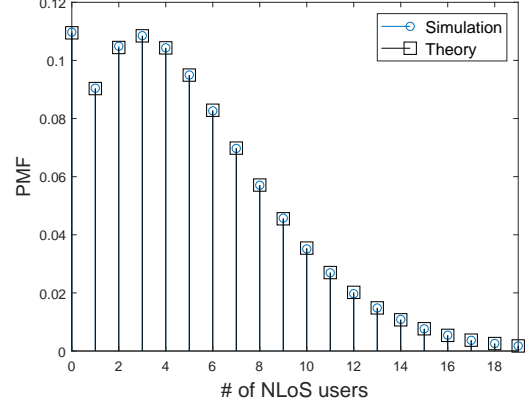


Fig. 7. The distribution of the number of NLoS users within a RSU cell whose size is selected to give an SNR equal to -6 dB at the cell edge. For the rest of the parameter settings see the caption in Fig. 6.

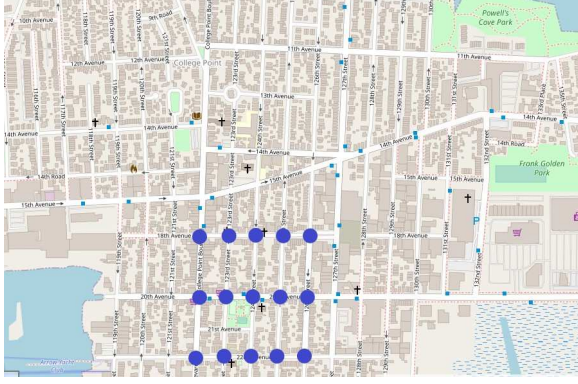
load distribution. Since the NLoS vehicles have much lower link gains than the vehicles along the typical lines L_x, L_y , the RSU must allocate to them more spectral resources under some fair scheduling scheme. Therefore our ability to quickly characterize the network load distribution for NLoS vehicles, see Fig. 7 for an example illustration, is important.

D. Model validation with a real map

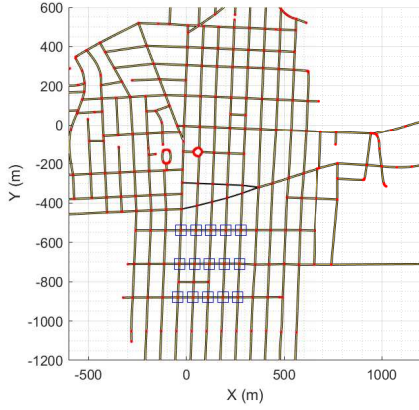
In this section, we investigate the effectiveness of the proposed approach in a practical setting, where the layout of the road network does not precisely follow the MPLP. For this purpose, we have extracted the road network of an urban area of size 1.8 km^2 using [36], [37], and selected 15 points, forming approximately a grid, where the distance distributions of the shortest paths are simulated. The map of the area can be seen in Fig. 8a and the associated road network in Fig. 8b. The extracted road network consists of approximately 500 linear segments. We assume that the locations of facilities follow a one-dimensional PPP of intensity λ_g along each segment. Therefore the only difference between the model and the studied scenario is the underlying road layout.

In Fig. 9a, we can see that the performance accuracy of Algorithm 1 improves for larger k , while, on the other hand, the prediction accuracy of the two-dimensional PPP degrades. In addition, increasing the density of facilities to $\lambda_g = 1 \text{ km}^{-1}$, compare Fig. 9a with Fig. 9b for the same value of k , is associated with worse model performance. That is because, for denser facilities, the k nearest neighbors are likely to come closer to the intersection points. As a result, the characteristics of the road network near the intersection points, which do not follow exactly the MPLP model, start to affect more.

We conclude this section by evaluating the model performance for a very low density of facilities. In this case, we use only the intersection point at the top-right corner of the grid located near the center of the total area. It can be considered that this point best represents the distance distributions in large urban areas, which, unfortunately, we do not have access to available data. We can see in Fig. 10 that the model performance further improves. The facilities spread out far from



(a) <https://www.openstreetmap.org/>



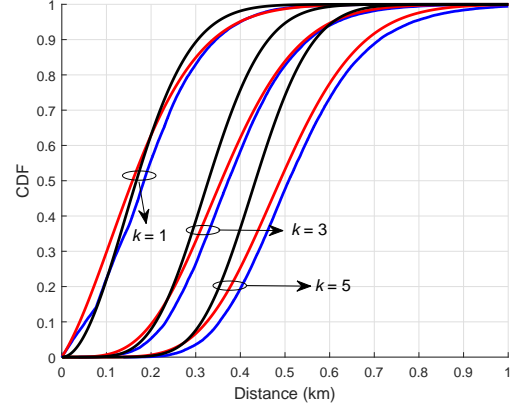
(b) <https://www.mathworks.com/products/automated-driving.html>

Fig. 8. (a) The map of an area near Manhattan, New York (40.7841/-73.8430). (b) The associated road network is extracted using Matlab toolboxes. All two-dimensional coordinates representing the start and the end points of road segments, generated by parsing the OpenStreetMap file, are depicted in red dots. The 15 intersection points where the shortest paths are simulated are depicted as blue squares; these points are illustrated as blue disks in Fig. 8a. The total length of streets in the considered area is approximately 40 km.

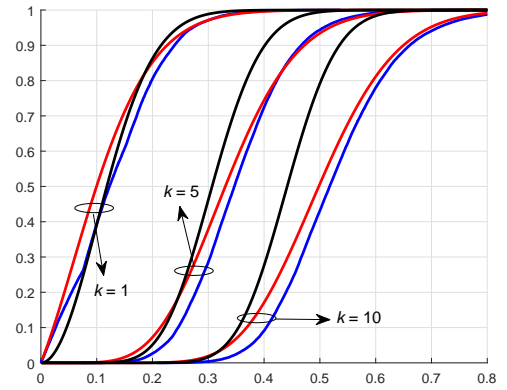
the intersection point, hence, the underlying road structure starts to have less effect on the path distance separation. That is a promising finding because it indicates that, for sparse facilities, the suggested model is fairly valid independently of the underlying urban road layout. However, further data collection from different cities is required to ascertain this finding.

VII. CONCLUSIONS

In this paper, we have devised a low-complexity numerical algorithm to calculate the distribution of the path distance between a randomly selected road intersection and the k -th nearest node of a Cox point process driven by the Manhattan Poisson line process. This algorithm can be used to identify the minimum required density of facilities (modeled by a MPLCP), e.g., charge stations for electric vehicles, to ensure that a vehicle at an intersection can reach the nearest available facility within a target time under a probability constraint. The distance distributions derived in this paper can also be used to calculate the distribution of network load within a cell of a V2X system. Finally, using real road network data, we illustrated the enhanced performance of the MPLP as



(a) $\lambda_g = 0.5 \text{ km}^{-1}$



(b) $\lambda_g = 1 \text{ km}^{-1}$

Fig. 9. Shortest path distance distributions for different intensities of facilities λ_g on a real map for 15 intersection points, see Fig. 8a. Near the intersection points, the intensity of horizontal streets is $\lambda_h \approx 5.9 \text{ km}^{-1}$ and the intensity of vertical streets is $\lambda_v \approx 12.5 \text{ km}^{-1}$ yielding $\lambda \approx 7.9 \text{ km}^{-1}$, which is used in Algorithm 1. 'Blue' lines are simulations, 'red' lines correspond to the MPLCP model (Algorithm 1) and 'black' lines to the two-dimensional PPP model, see equation (21). 2 500 simulation runs per intersection point. In each run an independent realization of facilities with the specified intensity λ_g is generated along every street segment. Then the shortest path distances are calculated using the Dijkstra algorithm.

compared to the state-of-art distance distribution model using the two-dimensional PPP. It is straightforward to incorporate into our approach path distance distributions towards a specific direction, e.g., south, north-east, etc. In the future, it would be interesting to extend our analysis and data collection with larger maps and different urban areas, investigating the independence of the path distance distributions from the underlying road infrastructure, when the network of facilities is sparse.

REFERENCES

- [1] G. Karagiannis, *et al.*, "Vehicular networking: A survey and tutorial on requirements, architectures, challenges, standards and solutions," *IEEE Commun. Surveys Tut.*, vol. 13, no. 4, pp. 584-616, Jul .2011.
- [2] D. Papadias, J. Zhang, N. Mamoulis and Y. Tao. "Query processing in spatial network databases," in *Proc. 29th Annu. Int. Conf. Very Large Databases*, Berlin, Sept. 2003, pp. 802-813.
- [3] C.S. Jensen, J. Kolár, T.B. Pedersen and I. Timko, "Nearest neighbor queries in road networks," in *Proc. 11th Annu. Int. Conf. Advances Geographic Inform. Syst.*, New York, ACM Press, 2003, pp. 1-8.

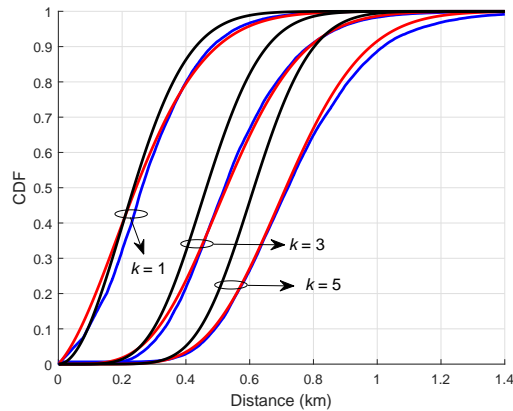


Fig. 10. Path distance distributions for the intersection point at the top-right corner of the grid of the 15 intersection points, see Fig. 8a. Intensity of facilities $\lambda_g = 0.25 \text{ km}^{-1}$. For the rest of the parameter settings, see the caption of the previous figure.

- [4] K. Mouratidis, M.L. Yiu, D. Papadias and N. Mamoulis, "Continuous nearest neighbor monitoring in road networks," in *Proc. 32nd Annu. Int. Conf. Very Large Databases*, Sept. 2006, pp. 43-54.
- [5] H. Hua, H. Xie and E. Tanin, "Is Euclidean distance really that bad with road networks?" in *Proc. 26th Annu. Int. Conf. Advances Geographic Inform. Syst.*, Seattle, ACM Press, Nov. 2018, pp. 11-20.
- [6] R.C. Thomson and D.E. Richardson, "A graph theory approach to road network generalization," in *Proc. 16th Int. Cartographic Conf.*, Barcelona, pp. 1871-1880, 1995.
- [7] S. Marshall, *et.al.*, "Street network studies: from networks to models and their representations," *J. Networks and Spatial Econ.*, vol. 18, pp. 735-749, 2018.
- [8] D.E. Knuth. Art of Computer Programming, Volume 3: Sorting and Searching. Addison-Wesley publishing, pp. 780, 1998.
- [9] N. Wei, J.L. Walteros and R. Batta, "On the distance between random events on a network," Wiley publishing, *Networks*, vol. 75, no. 2, pp. 203-231, Nov. 2019.
- [10] M. Barthélemy, "Spatial Networks," *Elsevier Physics Reports*, vol. 499, no. 1-3, pp. 1-101, 2011.
- [11] S.N. Chiu, D. Stoyan, W.S. Kendall and J. Mecke. Stochastic geometry and its applications. John Wiley & Sons Ltd., ISBN: 978-0-470-66481-0, 2013.
- [12] J.G. Andrews, F. Baccelli and R.K. Ganti, "A tractable approach to coverage and rate in cellular networks," *IEEE Trans. Commun.*, vol. 59, pp. 3122-3134, Nov. 2011.
- [13] C.S. Choi and F. Baccelli, "Poisson Cox point processes for vehicular networks," *IEEE Trans. Veh. Technol.*, vol. 67, pp. 10160-10165, Oct. 2018.
- [14] —, "Analytical framework for coverage in cellular networks leveraging vehicles," *IEEE Trans. Commun.*, vol. 66, pp. 4950-4964, Oct. 2018.
- [15] V.V. Chetlur and H.S. Dhillon, "Coverage analysis of a vehicular network modeled as Cox process driven by Poisson line process," *IEEE Trans. Wireless Commun.*, vol. 17, pp. 4401-4416, Jul. 2018.
- [16] —, "Success probability and area spectral efficiency of a VANET modeled as a Cox process," *IEEE Wireless Commun. Lett.*, vol. 7, pp. 856-859, Oct. 2018.
- [17] K. Koufos and C.P. Dettmann, "Distribution of cell area in bounded Poisson Voronoi tessellations with application to secure local connectivity," *J. Statistical Physics*, vol. 176, pp. 1296-1315, 2019.
- [18] —, "Temporal correlation of interference and outage in mobile networks over one-dimensional finite regions," *IEEE Trans. Mobile Comput.*, vol. 17, pp. 475-487, Feb. 2018.
- [19] R.Z. Ríos-Mercado, "Optimal districting and territory design," *Springer Int. Publishing*, <https://doi.org/10.1007/978-3-030-34312-5>, 2020.
- [20] ETSI EN 302 637-2 V1.3.1. Intelligent Transport Systems (ITS); Vehicular Communications; Basic Set of Applications; Part 2: Specification of Cooperative Awareness Basic Service. Sept. 2014.
- [21] ETSI TR 103 562 V2.1.1. Intelligent Transport Systems (ITS); Vehicular Communications; Basic Set of Applications; Analysis of the Collective Perception Service (CPS); Release 2. Dec. 2019.
- [22] J.P. Jeyaraj and M. Haenggi, "Reliability analysis of V2V communications on orthogonal street systems," in *Proc. IEEE Global Commun. Conf. (Globecom)*, Singapore, Dec. 2017, pp. 1-6.
- [23] K. Koufos and C.P. Dettmann, "The meta distribution of the SIR in linear motorway VANETs," *IEEE Trans. Commun.*, vol. 67, pp. 8696-8706, Dec. 2019.
- [24] —, "Outage in motorway multi-lane VANETs with hardcore headway distance using synthetic traces," *IEEE Trans. Mobile Comput.*, to be published.
- [25] —, "Moments of interference in vehicular networks with hardcore headway distance," *IEEE Trans. Wireless Commun.*, vol. 17, pp. 8330-8341, Dec. 2018.
- [26] F. Baccelli and X. Zhang, "A correlated shadowing model for urban wireless networks," in *Proc. IEEE Conf. Comp. Commun. (Infocom)*, Hong Kong, Apr./May 2015, pp. 1-9.
- [27] J.P. Jeyaraj and M. Haenggi, "Cox models for vehicular networks: SIR performance and equivalence," to be published, *IEEE Trans. Commun.*, DOI 10.1109/TWC.2020.3023914.
- [28] Y. Wang, K. Venugopal, A.F. Molisch and R.W. Heath, "MmWave vehicle-to-infrastructure communication: Analysis of urban microcellular networks," *IEEE Trans. Veh. Technol.*, vol. 67, pp. 7086-7100, Aug. 2018.
- [29] D. Evans, A.J. Jones and W.M. Schmidt, "Asymptotic moments of near-neighbour distance distributions," in *JSTOR Proc. Math., Physical Eng. Sci.* vol. 458, no. 2028, pp. 2839-2849, Dec. 2002.
- [30] D. Molchanov, "Distance distributions in random networks," *Elsevier Ad Hoc Networks*, vol. 10, no. 6, pp. 1146-1166, 2012.
- [31] M. Afshang and H.S. Dhillon, "Fundamentals of modeling finite wireless networks using binomial point process," *IEEE Trans. Wireless Commun.*, vol. 16, pp. 3355-3370, May 2017.
- [32] Z. Khalid and S. Durrani, "Distance distributions in regular polygons," *IEEE Trans. Veh. Technol.*, vol. 62, pp. 2363-2368, Jun. 2013.
- [33] V.V. Chetlur, H.S. Dhillon and C.P. Dettmann, "Shortest path distance in Manhattan Poisson Line Cox Process," *J. Statistical Physics*, under minor revision. Available online: arxiv.org/abs/1811.11332.
- [34] H.S. Dhillon and V.V. Chetlur. Poisson Line Cox Process: Foundations and Applications to Vehicular Networks. Morgan & Claypool, Jun. 2020.
- [35] W.P. Johnson, "The curious history of Faà di Bruno's formula," *The Mathematical Association of America*, Monthly 109, Mar. 2002.
- [36] OpenStreetMap contributors, <https://www.openstreetmap.org>
- [37] I. Filippidis, OpenStreetMap Functions, <https://github.com/johnyf/openstreetmap>, GitHub. Retrieved January 5, 2021.
- [38] M. Haenggi, "On distances in uniformly random networks," *IEEE Trans. Inf. Theory*, vol. 51, pp. 3584-3586, Oct. 2005.
- [39] J.B. Andersen, T.S. Rappaport, and S. Yoshida, "Propagation measurements and models for wireless communications channels," *IEEE Commun. Magazine*, vol. 33, pp. 42-49, Jan. 1995.